

Global Causal Structure of a Transient Black Object

Tehani Finch ^{*} and James Lindesay [†]
 Computational Physics Laboratory
 Howard University, Washington, D.C. 20059

Abstract

A singularity-free and spherically symmetric transient black object whose center remains always timelike, yet directly manifests a trapped region, has been constructed and numerically implemented. The exterior geometry is shown to be similar to that of a long-lived transient black hole, with a few subtle differences. The large-scale global structure of the geometry is examined through the construction of a conformal diagram, which exhibits no event horizon and bears resemblance to that of a Minkowski spacetime. Since there is no singularity within the geometry, the evolution of the exchange of information between timelike observers, including those that fall through the trapped region, can be directly explored. The dynamics of generic “standard” communications, as well as entangled communications, is exhibited through both t vs. r and conformal spacetime diagrams.

1 Introduction

Quantum aspects of gravitating systems continue to be actively explored in the physics literature. Cosmologies with trapping surfaces are of particular interest, since the geometry presents regions of interplay between quantum and gravitational phenomena. In particular, black holes manifest horizons, which are lightlike surfaces bounding regions of information exchange. For black holes, the very coupling of geometrodynamics to quantum processes likely implies that descriptions of the spacetime should qualitatively differ from classical static systems. For instance, any temperature associated with a static black hole generates radiations that modify the black hole. Furthermore, the classical, static horizon of Schwarzschild geometry is a $t = \infty$ surface, implying that those exterior to the horizon can never observe infalling objects reach it. However, infalling energies likewise modify the dynamic surfaces through which they fall. Therefore, geometries with explicit time dependence are needed to model dynamic spacetimes consistent with actual systems.

^{*}e-mail address, tkfinch@howard.edu

[†]e-mail address, jlindesay@fac.howard.edu

To gain further insights into the surfaces generated in dynamic cosmologies, dynamic black holes embedded in asymptotically Minkowski spacetimes have been developed and explored [1, 2]. The metric forms utilize non-orthogonal coordinates inspired by river models of stationary spacetimes [3], with a temporal dependency parameterized by the river time rather than the Schwarzschild time. The geometries are free of singularities away from $r = 0$. Fixed temporal coordinate curves remain spacelike surfaces throughout the dynamic geometries, corresponding to the times measured by certain inertial observers. The motivation for developing these dynamic descriptions is that such a temporal foliation simplifies one’s descriptions of quantum coherent processes on the geometry. Those inertial observers satisfying $u_{obs}^{ct} = 1$ have been referred to as being *geometrically stationary* [4], and in Robertson-Walker cosmology such observers are usually called *co-moving* observers. These qualitative differences from Schwarzschild time make examinations of quantum behaviors and information dynamics on such geometries more straightforward.

The results presented will develop as follows. In Section 2, the geometry of an example spherically symmetric transient black object is developed. Its stress-energy densities will depend upon time and radial coordinates, and will satisfy all energy conditions everywhere during accretion, and in the exterior during evaporation. Consistency conditions on the geometry are demonstrated, and lightlike trajectories within and near the trapped region are explored. Section 3 develops the conformal diagram of the dynamic spacetime, demonstrating global causal properties of the singularity-free and horizon-free geometry. To complete the discussion, Section 4 then examines the recovery of information temporarily trapped within the transient black object. The temporal and kinematic dynamics of the outgoing communications of an infalling emitter are displayed via spacetime diagrams and plots of emission rates. The evolution of an entangled photon pair, one of which traverses the trapped region, is also explicitly demonstrated.

2 Transient Black Objects

Because of their relative mathematical simplicity, static black holes have been of considerable interest in the study of quantum mechanics in gravity, as well as their influence upon the formative dynamics of galaxies. An uncharged, spherically symmetric black hole has a spacelike “center” $r = 0$ that implies the existence of a horizon. This horizon delineates the outermost boundary of a region of spacetime within which all future-trending trajectories ultimately hit the “center.” However, it is possible to construct a geometry that behaves very similarly to a transient black hole in the exterior, but has an innermost boundary to the trapped region, for which all causal trajectories have decreasing radial coordinate [5, 6]. The innermost region then serves as a “depository” that temporarily stores any information that falls into the region of trapped trajectories. The development of

such a transient black object will be the subject of this section.

2.1 Form of the metric

The radially dynamic spacetime metric for a spherically symmetric, temporally transient black object will be developed from the general metric

$$ds^2 = -\left(1 - \frac{R_M(ct, r)}{r}\right) (dct)^2 + 2\sqrt{\frac{R_M(ct, r)}{r}} dct dr + dr^2 + r^2 d\theta^2 + r^2 \sin^2\theta d\phi^2, \quad (2.1)$$

whose properties and virtues have been discussed in [1, 7]. In this equation, a finite radial mass scale $R_M(ct, r) \equiv 2G_N M(ct, r)/c^2$ is a length scale of the mass-energy content of the black object, $G^0_0 = \frac{1}{r^2} \frac{\partial}{\partial r} R_M(ct, r) = -\frac{8\pi G_N}{c^4} T^0_0$. The metric takes the form of Minkowski spacetime both asymptotically ($r \gg R_M$) as well as when the radial mass scale vanishes.

Radial trajectories for test particles of mass m in this geometry have 4-velocity components that satisfy

$$u^r = -\sqrt{\frac{R_M}{r}} u^{ct} \pm \sqrt{(u^{ct})^2 - \Theta_m} \quad , \quad \Theta_m \equiv \begin{cases} 1 & m \neq 0 \\ 0 & m = 0 \end{cases} \quad , \quad (2.2)$$

where the + sign signifies “outgoing” trajectories, and the - sign signifies “ingoing” trajectories. For massive systems whose proper time (up to an additive constant) is given by t , the temporal component of their 4-velocities satisfy $u^{ct} = 1$, and the trajectory is neither ingoing nor outgoing. Freely falling trajectories sharing this temporal coordinate represent what have been referred to as *geometrically stationary* trajectories [4]. For this physical setting, observer trajectories with 4-velocity components satisfying $u^{ct}_{obs} = 1$, $u^r_{obs} = -\sqrt{\frac{R_M}{r_{obs}}}$ can be shown to satisfy geodesic equations for massive gravitating systems which share proper time with the asymptotic observer, $dt = d\tau$. These are the co-moving observers of this geometry.

The radial coordinate provides the length scale for local angular proper distances $d\ell_\theta = r d\theta$ and transverse areas $d^2\sigma = r^2 \sin\theta d\theta d\phi$. One should also note that any geometrically stationary observer ($u^{ct} = 1$) in this geometry will measure a proper radial distance interval at a fixed time value (i.e. a synchronous proper length measurement shared by other geometrically stationary observers) given by $ds = dr$. This implies that r can also be interpreted as the proper distance between a geometrically stationary observer with coordinates (ct, r) and that geometrically stationary observer that is encountering the center $r = 0$ at the same value of t . This fact motivates the use of the term “center” for $r = 0$ [8]. Such an interpretation does not hold for fiducial (fixed r) observers, who must undergo accelerations in order to maintain their radial coordinate.

As can be seen from (2.1) and (2.2), at the *trapping surfaces* R_{TS} , instantaneously given by solutions to

$$1 = \sqrt{\frac{R_M(ct, R_{TS})}{R_{TS}}}, \quad (2.3)$$

outgoing light will be momentarily stationary. In addition, curves of fixed radial coordinate labeled by r are spacelike in the region between these surfaces. Thus, if solutions to this equation exist, the surfaces R_{TS} bound regions that exclude the possibility of having fiducial observers, since even light cannot be stationary within these regions. Such regions are referred to as *trapped regions* of the spacetime. If trapped regions exist, the geometry contains a “black object.” If there is a horizon, the geometry contains a “black hole.”

Several points of interest directly follow from these equations and the form of the metric:

- The radial coordinate is a proper distance as well as a measure of transverse areas for a class of observers;
- Outgoing photons at the trapping surface are momentarily stationary in the radial coordinate. For dynamic geometries, outgoing photons that are crossed by the outermost trapping surface have $u_{\gamma+}^r = 0$ at that instant. Thus, there can be no observers with stationary or increasing radial coordinate in regions for which $u_{\gamma+}^r \leq 0$. The radial scales R_{TS} represent *static limits* in this geometry. These surfaces are sometimes referred to as “apparent horizons”.

A calculation of curvature components for the metric (2.1) exhibits no inherent singularities away from $r = 0$. This means that no observer measures singular curvatures on any surface or transition time of the geometry. The functional form of the radial mass scale $R_M(ct, r)$ can also be chosen to preclude any singular behavior at $r = 0$ itself. Such geometries are thus singularity free.

It is quite straightforward to choose a form for the radial mass scale that generates a region in the spacetime for which the center $r = 0$ is spacelike, yet non-singular, generating a singularity-free black hole. However, for such a geometry, energy densities in the vicinity of the center are necessarily exotic, since their constituents cannot be timelike. Alternatively, one can directly develop dynamic geometries for which the center remains timelike perpetually, yet contain transient bounded trapped regions. The exterior of such a geometry behaves similarly to a transient black hole. It should be straightforward to examine unitarity and information dynamics everywhere since the spacetime is horizonless and singularity-free. Such a geometry, referred to henceforth as a *transient black object*, will be examined in what follows.

It should be noted that in certain circumstances, black objects within which the center remains perpetually timelike nevertheless develop horizons, thus also becoming black holes. For instance, if the black object does not evaporate away, a region develops within the object for which outgoing lightlike trajectories reach $t = \infty$, but not exterior lightlike future infinity, thus implying a horizon. Timelike trajectories interior to the trapped region cannot escape, but exterior observers can fall in and become trapped. However, one cannot have a *transient* black hole without developing a spacelike center $r = 0$. Therefore, the transient black object considered in this paper is distinct from a transient black hole in that the trapped information can be recovered in its “original” form in the future, in principle.

2.2 Accretion

One of the motivations for this model was the fulfillment of energy conditions over the broadest possible region of spacetime. Classical gravitating systems are expected to satisfy various energy conditions everywhere. However, quantum systems exhibit spacelike coherent behaviors, which can violate these conditions. Such violations are necessary for the evaporation of black holes [9].

The null energy condition (NEC) and weak energy condition (WEC) state that the quantity

$$\mathcal{I}_{null/weak} \equiv -u_{null/weak}^\mu T_{\mu\beta} u_{null/weak}^\beta \quad (2.4)$$

should be non-positive (*i.e.* $\mathcal{I}_{null/weak} \leq 0$), for lightlike (in the NEC case) and timelike (in the WEC case) observer 4-velocities, where $T_{\mu\beta}$ refers to the energy-momentum tensor. The dominant energy condition (DEC) refers to the 4-momentum p_{source}^μ of the matter distribution as seen by the observer with 4-velocity \vec{u}_{obs} , given by $p_{source}^\mu \equiv -T^\mu{}_\beta u_{obs}^\beta$. The DEC requires that this 4-momentum satisfy

$$\mathcal{I}_{observer}^{DEC} \equiv \vec{p}_{source} \cdot \vec{p}_{source} \leq 0 \quad (2.5)$$

for all observers, where the dot product is defined by the metric of the geometry. The DEC implies the WEC and NEC, so it provides the most significant constraint. Matter distributions that do not satisfy the DEC are described herein as “exotic.”

The dominant energy condition for this geometry is satisfied if

$$0 \leq \frac{\partial}{\partial ct} R_M(ct, r) \leq 2\sqrt{\frac{R_M(ct, r)}{r}} \frac{\partial}{\partial r} R_M(ct, r). \quad (2.6)$$

A solution to this non-linear relation satisfying the energy conditions, R_M^{EC} , is given by

$$R_M^{EC}(ct, r) = \frac{4}{9} \frac{r^3}{(ct_B - ct)^2}. \quad (2.7)$$

When substituted into Einstein's equation, this form generates a pressureless collapse of matter whose edge will be referred to as $r_{\text{exterior}}(ct)$. During accretion, the exterior surface satisfies the equation

$$R_M(ct, r = r_{\text{exterior}}) = R_{So} \equiv \frac{2G_N M}{c^2}, \quad (2.8)$$

where M denotes the total mass in the cosmology. R_{So} represents the Schwarzschild radius for a static geometry with mass M . Thus, during the period of accretion only,

$$R_M(ct, r) = \begin{cases} R_M^{EC}(ct, r) & \text{interior, } R_M^{EC}(ct, r) < R_{So} \\ R_{So} & \text{exterior, static vacuum.} \end{cases} \quad (2.9)$$

The exterior surface $r_{\text{exterior}}(ct)$ can be shown to collapse at a sub-luminal rate. The accretion will be assumed to continue until the exterior surface reaches a bounce scale L_{bounce} defined by micro-physics that will be described in the next subsection.

2.3 Evaporation

A region in spacetime within which any outgoing lightlike trajectory will have decreasing radial coordinate initiates once $R_M(ct_{\text{dark}}, r = R_{So}) = R_{So}$, *i.e.* the matter has collapsed within its Schwarzschild radius. This defines the time of the onset of a trapped region as t_{dark} . At that time, evaporation due to quantum effects is assumed to begin. However, the collapse will continue indefinitely unless some microscopic effect prevents complete degeneracy or the formation of a singularity. It will be assumed that such micro-physics contains a fundamental length scale limiting gravitational degeneracy. This finite, arbitrarily small, scale will be chosen here to have a fixed value L_{bounce} , beyond which microscopic pressures and quantum non-locality prevent further collapse. The functional behavior of R_M interior to L_{bounce} must then be of a form that prevents the formation of a singularity, *i.e.* such that $\text{Lim}_{r \rightarrow 0} \frac{R_M(ct, r)}{r} < \infty$. If this limit attains a value greater than unity, a horizon will form, creating a non-singular *black hole*. Otherwise, the center $r = 0$ will remain timelike everywhere, and if a trapped region forms, the geometry will manifest a generic *black object*. In the exterior, both types of dark geometries are quite similar prior to complete evaporation. Since there is no spacelike center, a sturdy system on a timelike trajectory can in principle be detected after evaporation of the black object.

The dynamics of information and the global causal structure of a dynamic black object is the subject of this investigation. During black object evaporation, the exterior region is delineated by the outermost trapping surface $R_S(ct)$, which is defined in terms of the interior mass of the the black object that has yet to evaporate

$$R_S(ct) \equiv \frac{2G_N M(ct)}{c^2}. \quad (2.10)$$

The dynamics describing the evaporation of this radial surface scale will be motivated using Hawking-like thermal radiation rates expected from a quasi-static geometry. The emission of such radiation from trapping surfaces has been discussed in the literature [10]. The rate of interior mass change is expected to be of the form

$$\dot{M}c^2 = \frac{\text{characteristic energy}}{\text{emitted quantum}} \times \frac{\text{number of quanta emitted}}{\text{unit time}},$$

where the dot indicates a derivative with respect to ct . The energy of the emitted quantum is expected to be defined by the spatial extent of the radial surface scale $R_S(ct)$, which likewise defines the temperature of a quasi-static geometry. For generality, an arbitrarily small additional microscopic scale δ_R will be included to prevent an indefinitely large energy, giving a form for this term of the order $\frac{\hbar c}{R_S(ct) + \delta_R}$. The rate of emission of the quanta for fiducial observers in the static geometry is expected to be of the order of one quantum per unit Rindler time [11], which is likewise inversely proportional to the radial surface scale. Again, for generality, an arbitrarily small microscopic scale δ_T will be added, resulting in a rate of emission $\frac{\kappa}{R_S(ct) + \delta_T}$, where κ is a dimensionless number of order one. Thus, multiplying by $\frac{2G_N}{c^2}$, the dynamics of the surface scale will be taken to satisfy

$$\dot{R}_S(ct) = - \frac{2L_{Planck}^2}{R_S(ct) + \delta_R} \frac{\kappa}{R_S(ct) + \delta_T}. \quad (2.11)$$

After the interior mass has decreased to a point where the radial surface scale is equal to the bounce scale L_{bounce} , the geometry no longer contains a trapped region, and the black object vanishes. Subsequently, all outgoing lightlike trajectories will have increasing radial coordinates. If there is no further quantum decay, a remnant of this mass will remain. However, for the present investigation, the core region will be assumed to continue quantum decay through massless quanta. The gravitationally stabilized quantum decay will be presumed to generate quanta that satisfy quantum measurement constraints as well as geometric consistency, as will be discussed shortly. During this decay, the exterior surface scale delineating the interior and exterior regions will take the fixed value L_{bounce} .[‡] The radial surface scale and the exterior surface scale are demonstrated in Figure 1. The particular form chosen for the decay is given by $R_S(ct) = A(ct - ct_{final})^2$, where $ct \leq ct_{final}$ and the constant A is chosen to smoothly match the final rate of thermal evaporation with the initial rate of decay. The quadratic form allows a smooth transition to Minkowski space.

[‡]Alternatively, if this scale were to maintain a time-dependent fractional value relative to $R_S(ct)$, the black object would continue thermal decay until all interior mass has evaporated. The development of such a model is quite straightforward, and its features do not exhibit significant modification from the model herein explored.

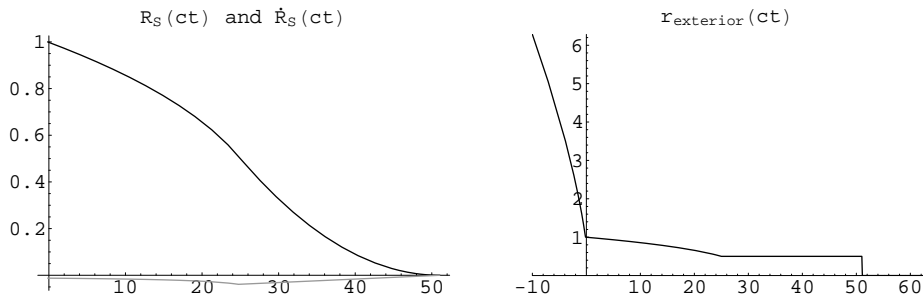


Figure 1: Plots of $R_S(ct)$ and $\dot{R}_S(ct)$ (left), and $r_{exterior}(ct)$ (right). The black curve on the left plot represents the radial surface scale, while the negative gray curve represents its derivative.

In the exterior region, changes in the interior mass will be presumed to be communicated via collections of massless quanta that carry energy and change the geometry. The quanta collectively carry sufficient energy to change the interior radial surface scale by δR_S , where $\delta R_S < 0$. The quanta then propagate through a static affine space with lesser interior radial surface scale $R_S + \delta R_S$. If this is done consistently, all energy conditions will be satisfied in the exterior.

Quantum measurement constraints can be estimated by examining the energy-at-infinity δE carried per emission by the outgoing quanta. The fact that $\delta R_S = \dot{R}_S \delta ct$, implies that $\delta E = -\frac{c^4}{2G_N} \delta R_S = \frac{\hbar c}{R_S(ct) + \delta R_S}$. Incorporating the uncertainty principle $\delta E \delta t \geq \frac{\hbar}{2}$ implies that the rate of decrease in the radial surface scale (for $\delta_R \simeq \delta_T$) has a lower limit given by $\delta R_S \delta ct_{emissions} > L_{Planck}^2$. However, there is also an upper limit upon the rate of evaporation/decay, due to geometric consistency and causality. Specifically the rate of thermal evaporation must be dynamically consistent so that energy carrying quanta do not leave spacetime flat enough that subsequent quanta eventually catch up. Indeed, a rapid enough evaporation would violate geometric consistency. The chosen decay form generates successive outgoing massless quanta that asymptotically have separations demonstrated in Figure 2. In the figure, geometry-changing quanta are emitted from the emission surface at small fixed intervals and propagated as outgoing quanta consistent with the metric (2.1) on null trajectories satisfying $\dot{r}_Q = 1 - \sqrt{R_M/r_Q}$.

Therefore, the specific model developed incorporates the following points:

- The geometry-changing quanta must emit exterior to the background radial surface scale R_S^{bg} through which they propagate, if they are to transport mass away;
- The geometry-changing quanta will thus propagate through a background geometry with surface scale $R_S + \delta R_S$ carrying energy $\delta E = -\frac{c^4}{2G_N} \delta R_S$;
- The emissions communicate the transport of energy as a lightlike outgoing

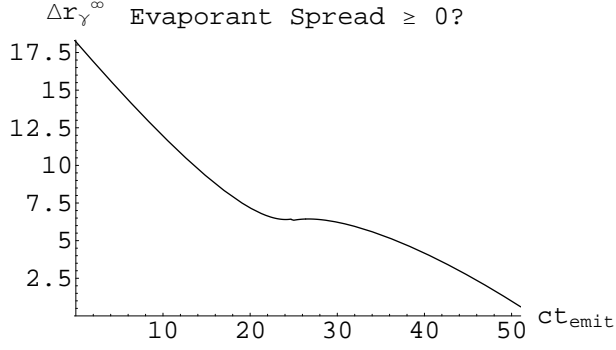


Figure 2: Asymptotic spread of sequentially emitted energy-carrying quanta.

energy that includes gravitational binding;

- Since the exterior radial mass scale incorporates the geometry-changing massless quanta, all energy conditions are expected to be satisfied in the exterior.

Each massless geometry-changing quantum “sees” a static geometry; it merely propagates through the geometry left behind by its immediate predecessor. Exterior outgoing quanta emitted at (ct_o, r_o) , located at $r_\gamma(ct)$, and propagating through a background geometry parameterized by R_S^{bg} satisfy

$$ct - ct_o = r_\gamma(ct) - r_o + 2\sqrt{R_S^{bg}}(\sqrt{r_\gamma(ct)} - \sqrt{r_o}) + 2R_S^{bg} \log \left(\frac{\sqrt{r_\gamma(ct)} - \sqrt{R_S^{bg}}}{\sqrt{r_o} - \sqrt{R_S^{bg}}} \right). \quad (2.12)$$

The geometry-changing quanta generated by evaporation or decay will thus propagate through a local background geometry characterized by $R_S^{bg}(ct_o) = R_S(ct_o) + \delta R_S(ct_o)$. In order to calculate the radial mass scale at an arbitrary exterior point (ct, r) , the retarded event of emission $(ct_o, r_o) \equiv (ct_{ret}, r_o(ct_{ret}))$ must be determined. During evaporation, the exterior emission scale will be chosen to satisfy $r_o(ct_{ret}) = R_S(ct_{ret}) + \delta_{stretch}$ (where $\delta_{stretch}$ can be arbitrarily small because the quanta propagate on a background of scale $R_S + \delta R_S$ as opposed to R_S itself).

The radial mass scale at a general exterior point will therefore be given by

$$R_M(ct, r) \equiv R_S(ct_{ret}(ct, r)) \quad , \quad r > r_{exterior}(ct) = R_S(ct). \quad (2.13)$$

This form then ensures a causal propagation of the evaporation of mass from the core region. During evaporation the core region is chosen to maintain its previous r -dependence from the accretion period, such that

$$R_M(ct, r) \equiv \frac{R_S(ct)}{R_S(ct_{dark})} R_M^{EC}(ct_{dark}, r) \quad , \quad r \leq L_{bounce} \quad (2.14)$$

where the pressureless form satisfying energy conditions R_M^{EC} is given by Eqn. (2.7). The region between the exterior and the bounce scale L_{bounce} will be assumed to maintain the spatially coherent form $R_S(ct)$. The chosen forms smoothly match the behaviors during the transition from accretion to evaporation.

As previously mentioned, this form for the radial mass scale has been chosen so as to satisfy energy conditions in the broadest region of the spacetime. Plots of the evolution of the radial mass scale, along with local measures of fulfillment of the energy conditions, are represented in Figure 3. The diagrams in the figure depict

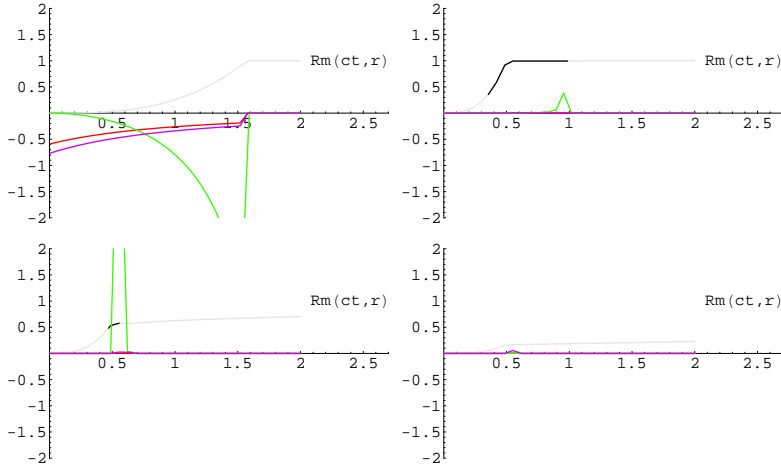


Figure 3: Radial mass scale and energy conditions for late accretion (upper left), final accretion with evaporation (upper right), mid-evaporation (lower left), and late decay (lower right). Both axes are measured in units of R_{S0} . The radial mass scale is shown in gray with a black overlay of trapped region. The DEC invariant $I_{observer}^{DEC}$ is shown for radial observer motions in red and for azimuthal observer motions in green. The NEC invariant \mathcal{I}_{null} is shown in purple. The energy conditions are satisfied for $I_{observer}^{DEC} \leq 0$ and $\mathcal{I}_{null} \leq 0$, respectively.

snapshots of these quantities during late accretion, the final stage of accretion after the black object has formed and evaporation has begun, the late stage of thermal evaporation, and the late stage of a gravitationally suppressed quantum decay of the remnant.

The gray curves in Figure 3 represent the spatial dependence of the radial mass scale at the given time. If there is a trapped region, it is represented by a black segment upon the radial mass scale curve. It is clear from the diagram that the trapped region has both an inner boundary R_{TS}^- and an outer boundary R_{TS}^+ . Curves are also demonstrated depicting local values for the DEC invariant $I_{observer}^{DEC}$ for radial observer motions (red), $I_{observer}^{DEC}$ for azimuthal observer motions (green), and the NEC invariant \mathcal{I}_{null} (purple), using a convention in which the DEC and NEC are satisfied when $I_{observer}^{DEC} \leq 0$ and $\mathcal{I}_{null} \leq 0$, respectively. All

energy conditions are everywhere satisfied prior to the beginning of evaporation, as expected. Also, energy conditions are satisfied everywhere in the exterior region $r > r_o(ct)$, implying that any measurements in the exterior will never detect exotic energy forms. The snapshots demonstrate violation of the energy conditions only within the region of spatial coherence where production of the quanta occurs. Such violations of energy conditions should be expected within the trapped regions, since these are also classically forbidden regions.

2.4 Construction of lightlike curves

The exploration of the dynamic features of a system is straightforward on a conformal diagram. Unfortunately, many useful dynamic geometries such as this transient black object do not afford a direct calculation of a set of conformal coordinates. A general technique is therefore necessary to construct Penrose diagrams in complicated geometries.

The technique relies only upon constructing lightlike surfaces for the given metric, in this case given in Eqn. (2.1). Once those null geodesics have been generated, the conformal coordinates can be labeled (v, u) , based upon the correspondence of the lightlike curves on reference hypersurfaces (in this case, the exterior surface and ultimately $skri^\pm$). Conformal spacetime coordinates (ct_*, r_*) can be introduced such that $v = ct_* + r_*$ and $u = ct_* - r_*$. For ingoing null geodesics, the required equation labeled by conformal coordinate v takes the form

$$\dot{r}_v = -1 - \sqrt{\frac{R_M}{r_v}}, \quad (2.15)$$

while outgoing null geodesics labeled by u satisfy

$$\dot{r}_u = 1 - \sqrt{\frac{R_M}{r_u}}. \quad (2.16)$$

For this geometry, ingoing lightlike trajectories labeled by v initiating on past lightlike infinity have access to all regions of spacetime. Outgoing lightlike trajectories labeled by u terminating on future lightlike infinity likewise have access to all regions of spacetime, since there is no horizon.

Ingoing lightlike trajectories defining the conformal coordinate v for the transient black object are demonstrated in Figure 4. The ingoing photons are chosen to terminate at $r = 0$, temporally separated in units of the Schwarzschild radius of the geometry R_{So} . For the chosen parameters, the trapped region first develops at $ct \simeq -0.167R_{So}$, and vanishes at $ct \simeq 25R_{So}$. Accretion ends at $ct \simeq +0.167R_{So}$, and final decay occurs at $ct \simeq 51.05R_{So}$. Ingoing photon trajectories are seen to propagate through essentially flat spacetime until they approach the trapped region, within which their radial coordinates decrease more rapidly

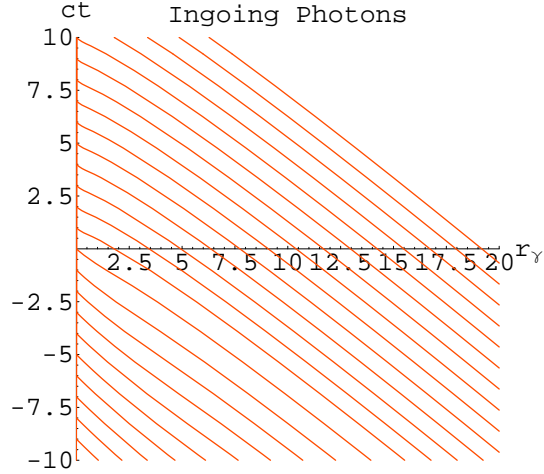


Figure 4: Ingoing lightlike trajectories. Results are displayed in units of R_{So} .

than in Minkowski spacetime. In the static exterior of the past, ingoing massless quanta satisfy

$$ct_o - ct = r_\gamma(ct) - r_o - 2\sqrt{R_{So}}(\sqrt{r_\gamma(ct)} - \sqrt{r_o}) + 2R_{So} \log \left(\frac{\sqrt{r_\gamma(ct)} + \sqrt{R_{So}}}{\sqrt{r_o} + \sqrt{R_{So}}} \right). \quad (2.17)$$

Thus, the outgoing lightlike surface of constant u communicating the beginning of evaporation can serve as the exterior surface of correspondence for assigning the parameter v during evaporation.

Outgoing lightlike trajectories defining the conformal coordinate u for the transient black object are demonstrated in Figure 5. The outgoing photons are emitted from $r = 0$, temporally separated in units of the radial mass of the geometry R_{So} . Photons emitted after the final decay of the black object propagate through flat spacetime. Likewise, photons emitted in the distant past propagate through nearly Minkowski spacetime. However, photons emitted just prior to the formation of the black object initially propagate with increasing radial coordinate, then have decreasing radial coordinate as the trapped region forms. Photons emitted during the lifetime of the black object (while there is a trapped region) also initially propagate with increasing radial coordinate, but slow as they approach the inner surface delineating the trapped region, being temporarily trapped within the innermost core region. It should be noted that *all* outgoing photons eventually will reach lightlike future infinity in this transient black geometry.

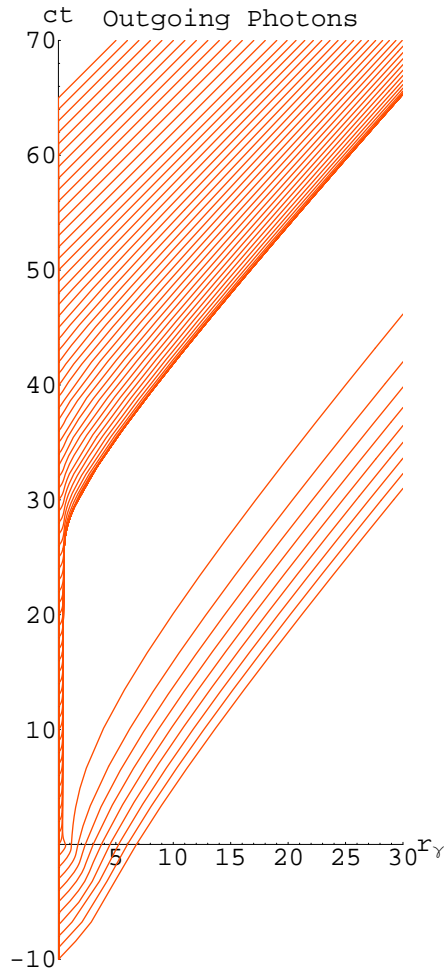


Figure 5: Outgoing lightlike trajectories (that originate at $r = 0$). Results are displayed in units of R_{S_0} .

3 Conformal diagram of the transient black object

Light-cone conformal coordinates ($v = ct_* + r_*$, $u = ct_* - r_*$) parameterized in the previous section will be made compact using the identification

$$\begin{aligned} Y_{\rightarrow} &= [\tanh(\frac{ct_*+r_*}{scale}) - \tanh(\frac{ct_*-r_*}{scale})]/2, \\ Y_{\uparrow} &= [\tanh(\frac{ct_*+r_*}{scale}) + \tanh(\frac{ct_*-r_*}{scale})]/2. \end{aligned} \tag{3.18}$$

The coordinates ($Y_{\rightarrow}, Y_{\uparrow}$) can be used to construct the Penrose diagram of this geometry with a transient black object. The geometry indeed has some finite period with real solutions of Eqn. (2.3) for the outer and inner surfaces of the trapped regions satisfying $R_{TS}^- \neq R_{TS}^+$, with the chosen parameters for the metric (2.1).

The conformal diagram, with significant transitional epochs indicated, is shown in Figure 6. The diagram is bounded from the left by the timelike center $r = 0$, from the lower right by past lightlike infinity $skri^-$, and from the upper right by future lightlike infinity $skri^+$. There are no horizons on the diagram. The static radial mass (Schwarzschild radius) of the geometry depicted by the (orange) curve labeled R_{So} sets the scale of the diagram. The center of the conformal coordinates ($Y_{\rightarrow} = 0, Y_{\uparrow} = 0$) is chosen to correspond with the coordinate ($ct = 0, r = R_{So}$). The timelike surface that delineates the exterior region of the geometry is depicted by the (red) dashed curve labeled R_X . During accretion, this curve represents the radial coordinate within which all mass in the spacetime is interior. After evaporation begins ($ct > ct_{dark} \approx ct_{bounce}$), R_X represents the radial scale within which mass that has yet to evaporate or decay away is contained. The spacelike surface showing the beginning of evaporation (ct_{dark}) is represented by the dashed (green) curve just prior to the solid (green) curve labeled ct_{bounce} in the diagram on the left. The latter depicts the end of accretion. The geometry-changing quanta emit from the surface labeled r_o , depicted by the black dashed curve. The dashed spacelike surface labeled $ct_{remnant}$ depicts the end of thermal evaporation, and the beginning of decay of the remnant. Finally, the solid (green) spacelike curve labeled ct_{final} depicts the end of decay of the remnant of evaporation. The region of the spacetime above the communication of the end of decay is flat. The diagram on the right demonstrates the boundaries of the trapped region.

Fixed-coordinate surfaces in the geometry are demonstrated in Figure 7. One of the most useful characteristics of this type of metric is that fixed-time coordinate surfaces are everywhere spacelike, and are shared by a set of geometrically stationary co-movers. This structure of the geometry is apparent in the figure. However, fixed-radius surfaces are also spacelike within the trapped region. In the diagram on the left, fixed-radius coordinate surfaces are everywhere timelike for $r > R_{So}$. Also, fixed-radius surfaces interior to the minimum value of the inner

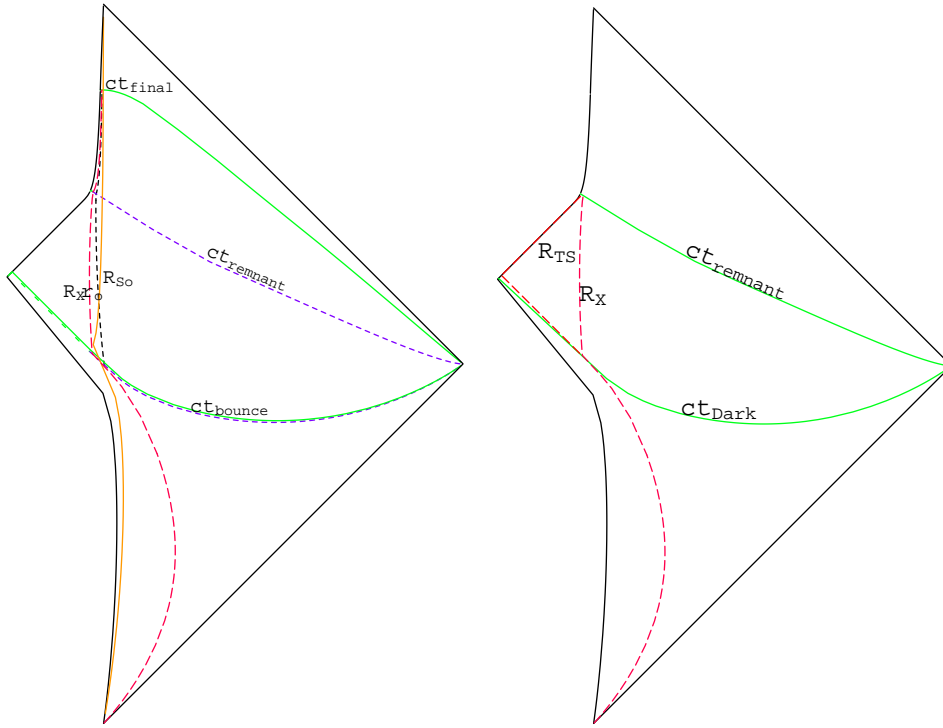


Figure 6: Conformal diagrams of the transient black object, demonstrating dynamic features of interest. The edge $r_{exterior}$ has been abbreviated R_X . The diagram on the right emphasizes the boundaries of the trapped region. Once the black object forms, the outer boundary R_X is always timelike, while the inner boundary R_{TS} is spacelike during evaporation.

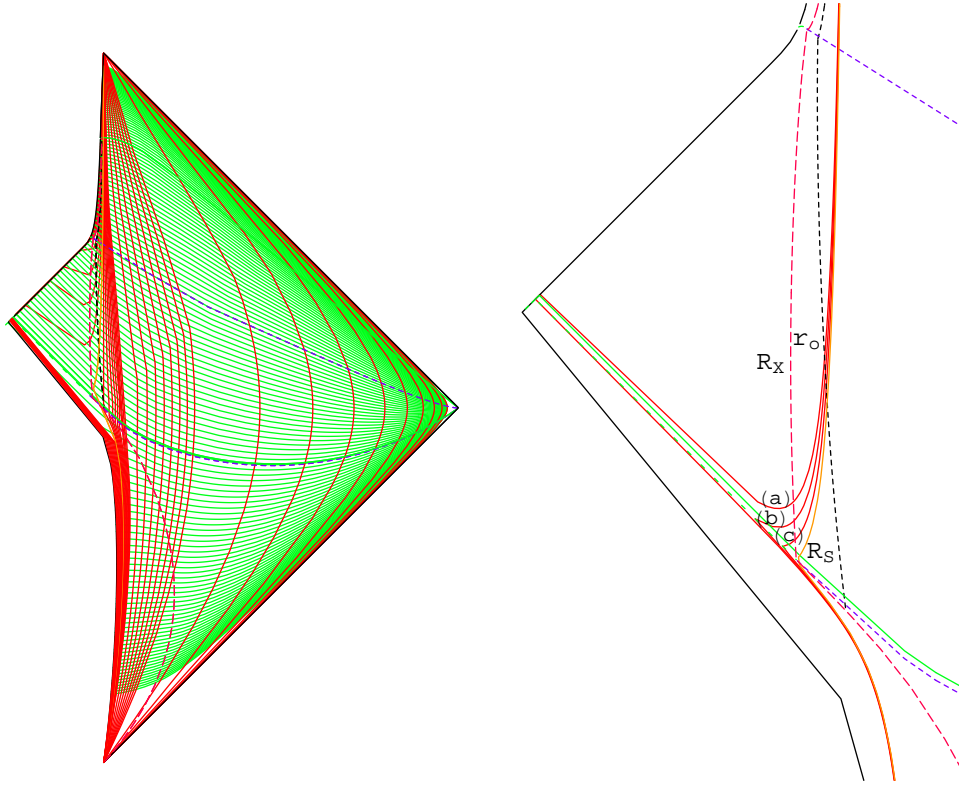


Figure 7: Fixed- ct and fixed- r surfaces on a conformal diagram for the transient black object. Left: Spacelike surfaces of fixed ct are represented by green curves graded in units of R_{S_0} . Curves of fixed radial coordinate r are represented by red curves graded in units of $0.1R_{S_0}$ from the center out to $2R_{S_0}$, then integral values of this unit, then decades of this unit. Right: Close-up view of (a) $r = 0.97R_{S_0}$, (b) $r = 0.98R_{S_0}$, and (c) $r = 0.99R_{S_0}$.

boundary of the trapped region $r < R_{TS}^-$ are always timelike, including the center $r = 0$. The boundaries of the trapped region represent surfaces for which outgoing lightlike trajectories are momentarily stationary in the radial coordinate. Those fixed-radius surfaces that lie within the trapped region demonstrate transition from timelike to spacelike, then back to timelike behaviors exhibited in the left-most region of the diagram. For clarity, this region is expanded in the diagram on the right of Figure 7. In this diagram, fixed-radius surfaces near the static mass scale R_{S_o} are depicted. The slope of each of the surfaces $r = \text{constant}$ is timelike prior to the formation of the black object, becomes unity as the innermost surface of the trapped region R_{TS}^- crosses that coordinate prior to the fixed-coordinate surface becoming spacelike, again becomes unity as the outermost surface of the trapped region $R_{TS}^+ = R_S(ct)$ crosses that coordinate, and is ultimately again timelike. This behavior has been observed in prior explorations of coordinate surfaces in transient trapped geometries [2, 8].

The behaviors of the outgoing null trajectories near the black object displayed in Figure 5 demonstrate that the outgoing communications from *any* system just before crossing the trapping surface are temporarily held near that surface. This is true for infalling systems at any time throughout the existence of the dynamic black object. However, all of these communications will eventually reach a nearby exterior observer after a finite time. In contrast, the analogous outgoing lightlike trajectories near a Schwarzschild horizon will release communications that only reach the exterior observer after an indefinitely long period of time. The next section will examine the dynamics of the release of these communications as systems enter the black object.

4 Dynamic information from trapped region-traversing observers

In order to examine the information dynamics of the transient black object, a standard exterior observer will be chosen to be geometrically stationary, thus sharing proper time with that of the asymptotic observer (t) parameterized in the metric. The initial conditions of this nearby observer can be chosen such that the observer avoids ever encountering the trapped region. This co-moving observer, whose trajectory is given by the outermost bold trajectory in Figure 8 will serve as the observational platform examining gravitating systems entering the trapped region. The trajectory was chosen to correspond to that of a stationary observer at $r = R_{S_o}$ after the remnant has completed its decay.

The observed infalling system will emit “standard” frequency photons at a “standard” rate in its proper coordinate frame of reference. In what follows, the emitter will be a freely falling, geometrically stationary system that reaches $r = R_{S_o}$ at time $ct = 10R_{S_o}$ (which is during evaporation), then falls through the

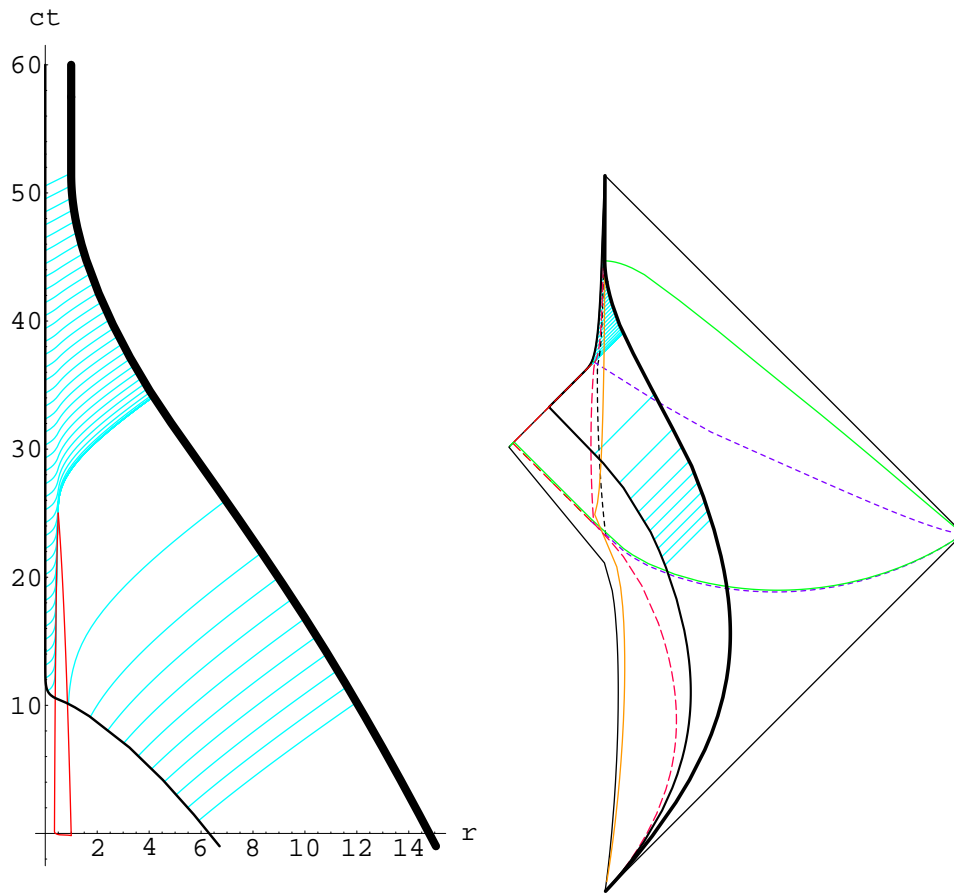


Figure 8: Standard photons that are emitted by a geometrically stationary in-falling source and detected by a nearby external observer. A standard spacetime diagram (which displays the boundaries of the trapped region) is represented on the left, and the conformal diagram is represented on the right.

trapped region. This infalling emitter is depicted by the innermost bold trajectory in Figure 8. The emitter approaches, but never reaches, the center $r = 0$. In the figure, the outgoing photons are emitted at $ct = R_{So}$, $ct = 2R_{So}$, $ct = 3R_{So}$, *etc.* There is an extended period of time during which only highly redshifted photons are observed from the emitter. This especially occurs between the communication of the emitter crossing into the trapped region and the communication of the end of the black object. After the emitter passes through the inner boundary of the trapped region, all outgoing communications are temporarily trapped inside that boundary, prevented from entering the trapped region. These photons “bunch up” within the inner surface of the trapped region, but are rapidly released after the trapped region vanishes, in a manner similar to that illustrated in Figure 5. Eventually, all emitted communications will be received by the observer.

4.1 Frequency shifts of quanta emitted by infalling emitters.

In order to examine the redshift of the emitted quanta, the null trajectories (2.16) that are obtained directly from the metric are not sufficient; the null geodesic equation

$$\frac{du^\beta}{d\lambda} + \Gamma_{\mu\nu}^\beta u^\mu u^\nu = 0, \quad (4.1)$$

is required (here λ is the affine parameter). The geodesic equation is used to calculate the 4-velocities for massless quanta. Subsequently, it is seen that the quantity $-\vec{u}_{obs} \cdot \vec{u}_\gamma$, the observed value of the temporal component of the 4-velocity of a radially outgoing photon, satisfies

$$-\vec{u}_{obs} \cdot \vec{u}_\gamma = \left(u_{obs}^{ct} \mp \sqrt{(u_{obs}^{ct})^2 - 1} \right) u_\gamma^{ct}, \quad (4.2)$$

where the \mp sign refers to outgoing/ingoing observers. This is directly proportional to the observed energy of the photon. For a geometrically stationary observer, $u_{obs}^{ct} = 1$, and the observed photon temporal component is seen to be simply u_γ^{ct} . The relationship (4.2) can likewise be used to express u_γ^{ct} in terms of its value $(u_\gamma^{ct})_{proper} = -\vec{u}_* \cdot \vec{u}_\gamma$ in the proper frame * of the emitter:

$$u_\gamma^{ct} = \frac{(u_\gamma^{ct})_{proper}}{u_*^{ct} \mp \sqrt{(u_*^{ct})^2 - 1}}, \quad (4.3)$$

where the \mp sign refers to outgoing/ingoing emitters. Since both the observer and the emitter are geometrically stationary, the geodesic equation directly calculates the observed frequency changes of the gravitating photons.

The rate of reception of information emitted from the infalling emitter can be obtained by examining the component u_γ^{ct} for the outgoing standard photons.

The standard frequency (in the frame of the source) for photons emitted will be chosen such that $u_{\gamma}^{ct}{}_{standard}=1$. The temporal behavior of u_{γ}^{ct} for standard photons from the infalling emitter *as measured by the geometrically stationary observer* is shown in Figure 9. The figure demonstrates both the evolution of the frequency

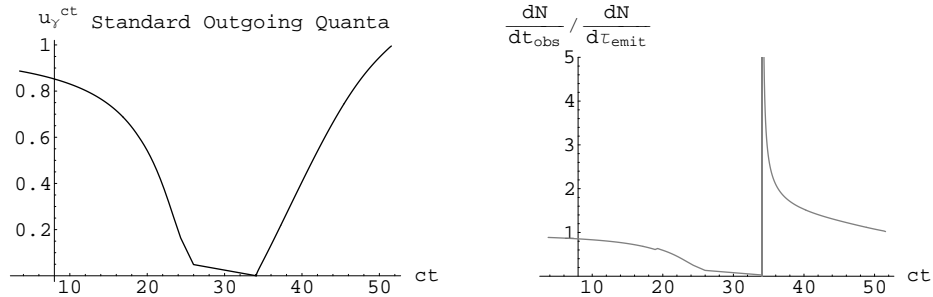


Figure 9: Left: Observed u_{γ}^{ct} of standard photons as a function of observation time. Right: Ratio of rate of observation of detected quanta to the rate of standard emission.

of individual photons on the left, as well as the rate of observation of photon emissions on the right. The rate of emission of photons is related to the interval $d\tau_{emit}$ between successive photons. Likewise, the interval between the observation of those successive photons by the co-moving observer dt_{obs} relates to the rate of detection. Thus, prior to the disappearance of the trapped region, the ratio of the rate of observation to the standard rate of emission should equal the ratio of the observed frequency to the standard frequency. As a check for numerical accuracy, this independent measure of redshift on the right of Figure 9 indeed functionally coincides with the geodesic calculation displayed on the left prior to the communication of the end of the black object. However, after communications from the emitter emerge following the evaporation of the trapped region, the individual photons depicted in the left diagram are initially quite redshifted and ultimately approach unit ratio from below, while the rate ratio in the diagram on the right is quite enhanced and ultimately approaches unit ratio from above. This should not be surprising, since such behavior is apparent in Figure 8.

The observation of infalling emitters through the trapped region of a transient black object is somewhat different from the observation of infalling emitters through the horizon of a transient black hole [8]. For emitters falling into transient black holes, any photons emitted by infalling systems before the horizon is crossed will continue to be redshifted until those systems are seen to completely vanish as the black hole itself fully evaporates away. This is true independent of the actual time that the system falls through the horizon, *i.e.*, all infalling emitters are seen to simultaneously vanish as they traverse the vanishing horizon of a transient black hole. However, for the transient black object, *all* emissions rapidly revert toward standard frequency and rate of emission as the trapped region evaporates.

For a static black hole, emitters are *never* observed to traverse the horizon (see, for instance, reference [11], page 23).

To complete this examination, a measure of the power of emissions from the infalling system as observed by the external observer will be developed. The power should be related to the energy of each photon times the rate at which photons are observed. This power parameter measured for radially outgoing photons at the radial coordinate of the external observer is displayed in Figure 10. After

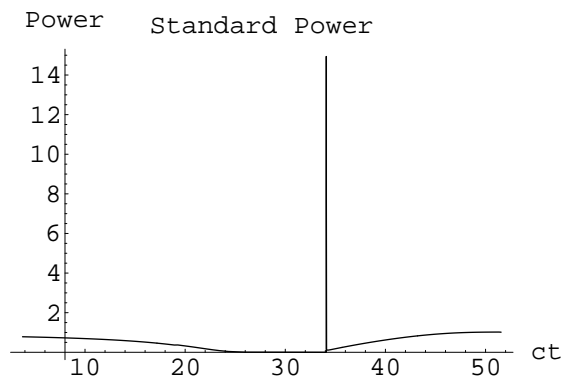


Figure 10: Normalized power $P_{standard}$ received by the geometrically stationary exterior observer.

final decay of the remnant, and for very early times, this standard power takes the value of unity. Just as the trapped region vanishes, there is a considerable spike observed in this measure of power.

If the detector used by a single external observer is small enough (or if there were an isotropic set of infalling emitters all radiating radially) the emissions are uniform over the observed solid angle. The actual detections are then expected to fall off with the inverse square of the radial distance traveled by the photon, which for a geometrically stationary emitter and observer is given by $r_{obs}(ct_{observed}) - r_*(ct_{emit})$. A diagram of this observed measure of “intensity” is demonstrated in Figure 11. Early measurements of this intensity are smaller than later measurements because of the greater distance between the emitter and the source. This intensity is normalized to take the value unity after the remnant has completely decayed. At this time, both the observer and system are motionless since geometrically stationary objects have fixed spatial coordinates in Minkowski spacetime. The figure demonstrates a spike in intensity as the trapped photons are released after the termination of thermal evaporation, which corresponds to the end of the black object.

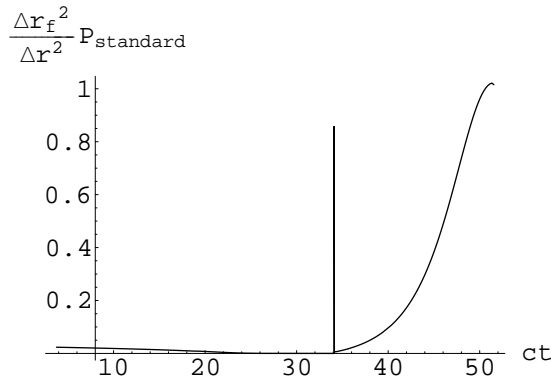


Figure 11: “Intensity” measured by the exterior observer using a small detector.

4.2 Entanglement of massless quanta.

The absence of a spacelike center for the singularity-free black object allows a direct exploration of the trajectories of gravitating entangled photons. As an example, consider a massive unstable particle coincident with the infalling geometrically stationary system that decays into an entangled pair of photons just as the particle encounters the outer trapping surface $R_S(ct_{decay})$. One of the photons will be emitted radially outward, and the other radially inward to conserve microscopic momentum. One observer (Alice) will be a geometrically stationary observer with final location $x = R_{S_o}$, while the other observer (Bob) will be a geometrically stationary observer located diametrically opposite the original observer with final location $x = -R_{S_o}$.

This arrangement is demonstrated in Figure 12. The left diagram of the figure is a spacetime plot using the coordinates (ct, x) , while the right diagram is a conformal plot derived from (ct, r) . The infalling unstable particle is represented by the dashed black curve, while the entangled photons which are the products of the decay are represented as the outgoing and ingoing null light-blue trajectories, ultimately detected by Alice and Bob. In the spacetime diagram on the left, the interior mass scale $R_S(ct)$, which coincides with the outer trapping surface while there is a black object present, is also demonstrated as a pair of solid (red) timelike curves slowly approaching zero.

The decay occurs just as the unstable particle encounters the trapping surface, indicated by the initial vertical slope of the outgoing photon trajectory that ultimately reaches Alice. The ingoing photon crosses the center, but remains trapped until the trapped region vanishes due to the evaporation of the black object, at which time it crosses the interior mass scale and ultimately is detected by Bob. In the radial conformal diagram on the right, Alice has azimuthal location $\phi = 0$, while Bob has azimuthal location $\phi = \pi$. Thus, these observations are actually

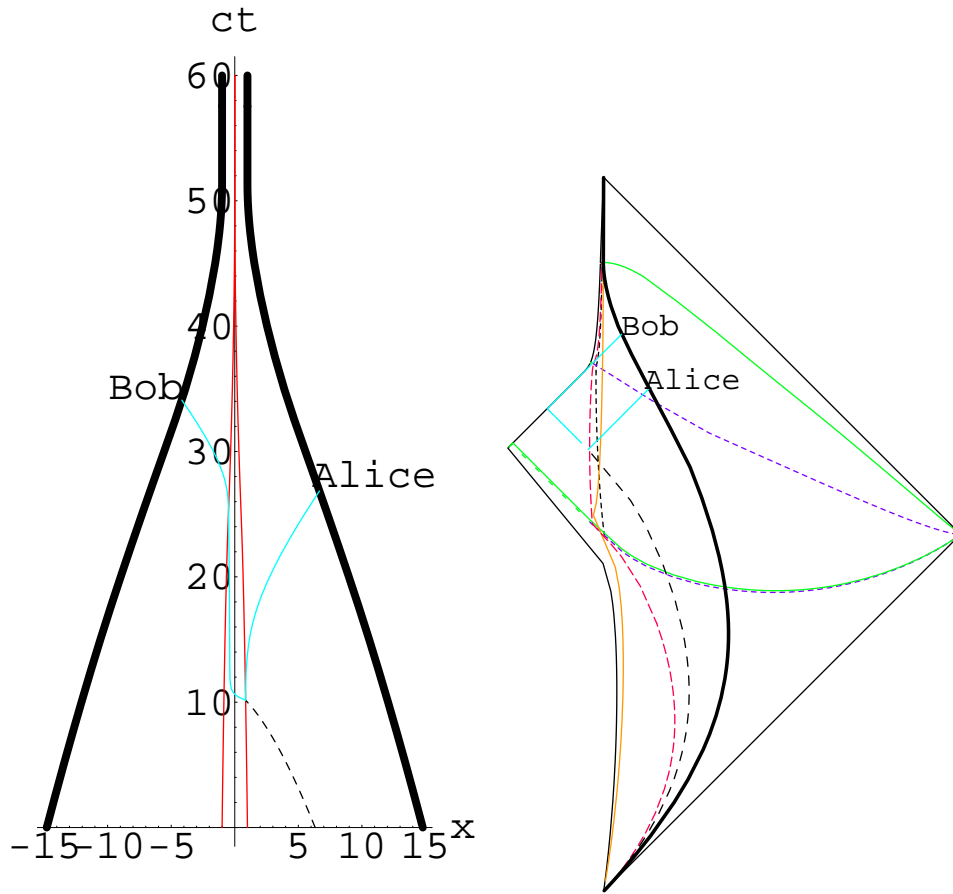


Figure 12: Trajectories of the entangled photon pair emitted by the unstable particle just as it crosses into the trapped region. The left diagram is a standard spacetime diagram using (x, ct) , while the right diagram utilizes conformal (radial) coordinates (Y_-, Y_+) and superposes two opposite values of the azimuthal angle ϕ .

spacelike separated, which is not depicted on the radially symmetric Penrose plot. In this diagram, the ingoing entangled photon “reflects” from the center as its polar angle switches from zero to π . It is interesting to note that, in contrast to the situation in flat spacetime, Alice and Bob likely detect the photons during differing epochs. In addition, the energy ratio $\epsilon \equiv \frac{u_{\gamma}^{ct}}{u_{\gamma^*}^{ct}}$ measured by Alice is $\epsilon \approx 0.01$, while that measured by Bob is $\epsilon \approx 8 \times 10^{-8}$. Thus, the spacetime and energy-momentum entanglement information measured by the different observers is both temporally-shifted and redshifted in energies.

5 Conclusions

A singularity-free transient black object whose center remains always time-like has been developed, and its evolution has been numerically explored. Such objects are difficult to distinguish from long-lived transient black holes in the exterior, yet are everywhere analytic. The geometry was constructed to satisfy energy conditions everywhere during accretion. In addition, the geometry satisfies energy conditions external to the trapped region, and external to any region expected to involve prolific production of quanta. The coordinates utilized are particularly useful since they admit a class of geometrically stationary (co-moving) observers. These observers share proper time with that of the asymptotic observer, directly parameterized by the metric time t . Geometrically stationary observers can serve as convenient platforms for performing measurements within the dynamic geometry.

The particular model explored involves a geometry with an overall energy distribution of fixed mass M that undergoes a pressureless collapse initiated in the distant past. The collapse terminates after quantum non-locality effects are presumed to dominate the dynamics [13]. Once mass is contained within a region smaller than its Schwarzschild radius, a trapped region (*i.e* a region in which all causal trajectories move toward decreasing radial coordinate) forms. However, since the center remains timelike and the black object is transient, no horizon develops, and the object never becomes a black hole. This collapsed black object then undergoes thermal decay analogous to that expected from a black hole until the trapped region vanishes. The remnant of thermal evaporation is then chosen to decay away in a manner consistent with quantum and geometric constraints.

A conformal diagram demonstrating the large-scale causal structure of the geometry has been demonstrated. The modification of the spacetime from that of Minkowski is minimal, since the center $r = 0$ remains everywhere timelike. In these coordinates, the development of a trapped region merely expands the volume of the conformal diagram, as expected from previous studies [8, 12]. Fixed-time surfaces remain everywhere spacelike, providing global foliation for parameterizing the dynamics. Surfaces of fixed radial coordinate have been demonstrated to be

timelike exterior to the trapped region, and spacelike within the trapped region.

Information exchange in the vicinity of the black object has also been explored. Outgoing photons from an infalling emitter were seen to redshift as the emitter approaches the trapped region. However, in contrast to a transient black hole, direct emissions that are temporarily trapped while the black object persists are later observed once the trapped region vanishes. This rapid release of information has been demonstrated for the model. The redshift of energies and the dynamics of the rate of communications are shown to behave as expected.

In order to explore the dynamics of entangled information, the trajectories of entangled photons have been examined. The photons were formed as a particle decayed while crossing into the trapped region. The presence of the transient black object alters the relative times of observation and energy redshifts of the entangled photons. The exploration directly demonstrates that the loss of entanglement information is only temporary for this geometry, and that there are no obvious cases of violation of the standard laws of physics.

The analytic and causal properties of this dynamic black object should considerably simplify the exploration of quantum geometrodynamics behaviors on the geometry, as will be demonstrated elsewhere [14]. Also, one should be able to incorporate such a transient black object within a dynamic de Sitter geometry consistent with big bang cosmology, as has been done with a transient black hole [8]. In principle, such a transient black object should introduce no exotic behaviors in the global geometry, while yet introducing an additional trapped region into the spacetime.

Acknowledgments

The authors warmly acknowledge their association with Beth Brown. TF is pleased to acknowledge past discussions with Ted Jacobson, along with support from Chanda Prescod-Weinstein. JL gratefully acknowledges useful past discussions with James Bjorken, Paul Sheldon, and Lenny Susskind.

References

- [1] Lindesay, J. (2007). “Coordinates with Non-singular Curvature for a Time-dependent Black Hole Horizon,” arXiv:gr-qc/0609019v2, 16 pages. *Foundations of Physics* **37** (2007), 1181-1196, online DOI: 10.1007/s10701-007-9146-4.
- [2] Lindesay, J. & Sheldon, P. (2010). “Penrose Diagram for a Transient Black Hole,” arXiv:1005.4449v2 [gr-qc], 14 pages. *Class.Quant.Grav.* **27** (2010), 215015.

- [3] Hamilton, A.J.S. & Lisle, J.P. (2008). “The River Model of Black Holes,” arXiv:gr-qc/0411060v2, 14 pages. *Am.J.Phys.* **76** (2008), 519-532, DOI: 10.1119/1.2830526.
- [4] Lindesay, J. (2009). “Quantum Behaviors on an Excreting Black Hole,” arXiv:0810.4515v1 [gr-qc], 33 pages. *Class.Quant.Grav.* **26** (2009), 125014 (24pp).
- [5] Hayward, S. (2006). “Formation and Evaporation of Non-singular Black Holes,” arXiv:gr-qc/0506126v2, 4 pages. *Phys.Rev.Lett.* **96** (2006), 031103.
- [6] Hossenfelder, S., Modesto, L., & Premont-Schwartz, I. (2010). “A Model for Non-singular Black Hole Collapse and Evaporation,” arXiv:0912.1823v3 [gr-qc], 7 pages. *Phys.Rev.* **D81** (2010), 044036.
- [7] Nielsen, A. & Visser, M. (2006). “Production and Decay of Evolving Horizons,” arXiv:gr-qc/0510083v3, 25 pages. *Class.Quant.Grav.* **23** (2006), 4637-4658.
- [8] Lindesay, J. & Finch, T. (2011). “Global Geometry of a Transient Black Hole in a Dynamic de Sitter Cosmology,” 40 pages. Accepted chapter, **Classical and Quantum Gravity: Theory, Analysis and Applications**, Vincent R. Frignanni, Editor. Nova Science Publishers, Inc. ISBN 978-1-61122-957-8 (2011).
- [9] Birrell, N.D. & Davies, P.C.W. (1982). **Quantum Fields in Curved Space**; Cambridge University Press: Cambridge, 1982, Chapter 8.
- [10] Visser, M. (2003). “Essential and Inessential Features of Hawking Radiation,” arXiv:hep-th/0106111v1, 17 pages. *Int.J.Mod.Phys.* **D12** (2003), 649-661.
- [11] Susskind, L. & Lindesay, J. (2005). **An Introduction to Black Holes, Information, and the String Theory Revolution: The Holographic Universe**; World Scientific: Singapore 2005.
- [12] Brown, B. A. & Lindesay, J. (2009). “Construction of a Penrose Diagram for an Accreting Black Hole.” arXiv:0811.0629v1 [gr-qc], 12 pages. *Class.Quant.Grav.* **26** (2009), 045010 (5pp) DOI: 10.1088/0264-9381/26/4/045010.
- [13] Lindesay, J. (2011). “Self-consistent Solutions of Canonical Proper Self-gravitating Quantum Systems”. arXiv:1108.4897v1 [gr-qc], 13 pages.
- [14] Lindesay, J. **Foundations of Quantum Gravity**; Cambridge University Press: expected to be published 2013.